INDIAN JOURNAL OF SCIENCE AND TECHNOLOGY

ORIGINAL ARTICLE

OPEN ACCESS

Received: 17/11/2025

Accepted: 27/11/2025

Published: 11/12/2025

Citation: Ponpandi RK, Mathavan A (2025) Exploration of the Preparative, Luminescent Characteristics, and Cellular Harmful Impact of Cerium-Enriched Cadmium Sulfide Nanoparticles. Indian Journal of Science and Technology 18(45): 3595-3607. https://doi.org/10.17485/IJST/v18i45.1791

* **Corresponding author**.

abhimathavan@gmail.com

Funding: None

Competing Interests: None

Published By Indian Society for Education and Environment (iSee)

ISSN
Print: 0974-6846
Electronic: 0974-5645

Exploration of the Preparative, Luminescent Characteristics, and Cellular Harmful Impact of Cerium-Enriched Cadmium Sulfide Nanoparticles

Ram Kumar Ponpandi[1†], **Alagarsamy Mathavan**[1*]

1 PG and Research Department of Chemistry, V.O. Chidambaram College, Tuticorin, 628008, Affiliated to Manonmaniam Sundaranar University, Abishekapatti, Tirunelveli, 627012, Tamil Nadu, India

Abstract

Objectives: The synthesis of pure and Cerium Doped CdS with the composition $Cd_{1-x}Ce_xS$ (where x = 0.001, 0.002, 0.003, and 0.004 %) was conducted to investigate the physical, structural, and optical properties of Ce-doped CdS. Method: Cerium-doped cadmium sulfide nanoparticles (Ce:CdS NPs) are synthesized using co-precipitation methods to control size, morphology, and optical properties. The band gap of these semiconductor nanoparticles was optimized through Diffuse Reflectance Spectroscopy (DRS). Crystallite size, microstrain, lattice parameter, and volume were characterized via X-ray diffraction (XRD). Emission properties were analyzed using photoluminescence spectroscopy (PL). Surface morphology and particle size were examined with Field Emission Scanning Electron Microscopy (FESEM). The surface functional groups were studied using Fourier Transform Infrared Spectroscopy (FTIR), while the chemical composition was evaluated through energy dispersive X-ray analysis (EDAX). The anticancer efficacy of Ce-doped nanoparticles was assessed with the MTT assay on a breast cancer cell line. Findings: In DRS spectra, higher dopant concentration leads to a reduced band gap, known as a red shift, suggesting new localized energy levels from Ce^{3+} ions in the CdS lattice. Increased cerium ion concentration results in an impurity band overlapping with the conduction or valence band edge of CdS. EDAX spectra show notable peaks like Cd-L, S-K, and Ce-K, confirming the presence of both pristine and doped nanoparticles. PL spectra indicate strong emission peaks in the visible region. FESEM analysis reveals cerium-doped nanoparticles typically have an irregular spherical distribution due to high surface energy. XRD studies indicate a phase transition from cubic to hexagonal structure at an optimal 4% cerium doping. The presence of larger cerium ions notably affects particle size,

[†]Research Scholar (Reg.No. 19122232031023)

lattice parameter, strain, and volume. FTIR spectroscopy identifies functional groups and capping agents in cetyl trimethylammonium bromide-assisted cerium-doped CdS nanoparticles. The spectrum displays characteristic peaks of CTAB alongside those of the inorganic core. Additionally, cerium-doped CdS nanoparticles demonstrate dose-dependent cytotoxicity, with increased concentrations decreasing cell viability, typically due to reactive oxygen species leading to oxidative stress and DNA damage. Novelty: Typically, cubic CdS nanoparticles demonstrate significant cytotoxic effects; however, it is noteworthy that for the first time, thermodynamically more stable hexagonal cerium-doped CdS nanoparticles exhibit superior anticancer activity in comparison to the standard therapeutic agent, doxorubicin.

Keywords: Red Shift; Cytotoxic effect; Hexagonal Ce doped CdS; Reactive oxygen species; MTT assay

1 Introduction

Cadmium sulfide (CdS) quantum dots (QDs) have garnered significant attention in the scientific community due to their exceptional optoelectronic characteristics, which make them highly desirable for various applications [(1)]. The presence of surface states or surface traps within these quantum dots can cause charge carriers that are generated inside the QDs to become localized at the surface. This phenomenon can unfortunately lead to an undesirable reduction in light emission, resulting in a marked decrease in the quantum yield of the QDs [(2)]. Specifically, cadmium-based (II-VI) semiconductor QDs, which include well-known varieties like cadmium selenide (CdSe), cadmium telluride (CdTe), and, of course, CdS, have been extensively studied not only for their high optical quantum yield but also due to their significant toxic effects on human health as well as aquatic life. The toxicity associated with these cadmium-based compounds has led to the implementation of various global regulations aimed at controlling and limiting their usage [(3)].

Furthermore, the doping of wide band-gap semiconductor QDs with rare-earth (RE) ions—excluding cerium—has proven to be quite a challenge. This is primarily due to the incompatibility of the ionic radius and charge state of rare-earth ions with the host lattices of II-VI semiconductors, which complicates the doping process. On the other hand, cerium-doped III-V semiconductor QDs exhibit a narrow emission peak when they are excited within the ultraviolet-visible spectral region. Notably, the position of this emission peak is adjustable depending on the manipulation of the size of the host quantum dot, allowing for fine-tuning based on specific application requirements [(4)], [(5)].

Inner transition elements (ITEs) like cerium, lanthanum, and uranium exhibit anticancer effects via five mechanisms: modulating reactive oxygen species (ROS), interacting with DNA, inhibiting enzymes, forming metal-based adducts, and changing signaling pathways. ITEs generate ROS, deplete antioxidants, and may cause cardiotoxicity. They non-covalently affect DNA transcription and replication, form alkyl adducts, inhibit DNA repair enzymes leading to cell death, and alter calcium fluxes and immune responses. [(6)], [(7)]

The extensive application of nanotechnology in the field of cancer therapy has significantly broadened in recent years with the remarkable development of advanced targeted delivery systems. In this innovative context, nanoparticles, particularly those based on cadmium sulfide (CdS) quantum dots, have the potential to function effectively as both cutting-edge imaging probes and powerful therapeutic agents. Furthermore, researchers are now able to thoroughly investigate the profound impact of plasmonic doping on various absorption characteristics and the intricate processes of photoluminescence. This exploration not only facilitates the selective observation of intricate cellular interactions but also contributes to the enhancement of overall diagnostic accuracy, paving the way for more precise and effective cancer therapies. [(8)], [(9)]

Metal doped metal chalcogenides quantum dots are a promising method for anticancer therapy. Usually, cubic CdS is well-documented for its connection to improved anticancer properties; however, it has been noted that hexagonal CdS nanoparticles have shown diminished effectiveness in combating cancer. On the contrary, our extensive research shows that hexagonal CdS nanoparticles actually exhibit higher anticancer activity than previously thought, which has been examined in detail and provides new insights into their potential benefits in cancer treatment. [(10)], [(11)] This study will cover the optical properties and anticancer effects of pure and Ce-doped CdS nanoparticles.

2 Methodology

2.1 Reagents

The nanoparticles incorporating Cerium, designated as CdS:Ce, have been synthesized utilizing a chemical co-precipitation method. Analytical grade Cerium Nitrate ($Ce(NO_3)_2 \cdot 6H_2O$), Cetyltrimethylammonium bromide (CTAB), Sodium Sulfide (Na_2S), and Cadmium Nitrate hexahydrate ($Cd(NO_3)_2 \cdot 6H_2O$) sourced from Sigma Aldrich were employed without additional purification processes. These analytical grade substances served as precursors for Cerium, stabilizing surfactant, sulfur, and cadmium, respectively. Each material was separately dissolved in double-distilled water to form the necessary precursors.

2.2 Chemical Synthesis of Pristine CdS and Ce doped CdS Nanoparticles

An aqueous solution of Cadmium Nitrate Tetrahydrate ($Cd(NO_3)_2 \cdot 4H_2O$) at a concentration of 0.1 M was prepared, amounting to approximately 100 mL, and stirred for a duration of one hour at room temperature. Subsequently, 100 mL of sodium sulphide (Na_2S) at the same molarity of 0.1 M was added gradually to the solution, followed by agitation using a magnetic stirrer for an extended period of 20 hours. Cetyltrimethylammonium bromide (CTAB) was employed as a capping agent to adjust the pH, facilitating precipitation reactions. A yellowish-orange precipitate was observed shortly after the addition of sodium sulphide. The solid and liquid phases of the resultant mixture were separated through centrifugation for 30 minutes at a rotational speed of 10,000 rpm. Contaminants were subsequently eliminated using ethanol, and the solution was thoroughly rinsed with sterile distilled water. The purified cadmium sulphide (CdS) nanoparticles were collected as pellets, which were then ground into a fine powder and subjected to calcination at a temperature of 250°C for one hour, thereby completing the synthesis and achieving crystallization. In order to synthesize 1% Ce:CdS Nanoparticles, 0.04 g (0.001 M) of rare earth element precursors was dissolved in 100 mL of ultrapure water within a beaker. Thereafter, 0.25 g of CTAB and 3.05 g (0.099 M) of $Cd(NO_3)_2$ were incorporated, and the mixture was stirred until homogeneity was attained. Solutions containing Cerium were prepared in a similar manner. Subsequently, sodium sulphide at a concentration of 0.1 M was introduced, and the resulting solution was maintained at a temperature of 70°C for duration of 24 hours [12]. The final product was then collected through centrifugation, washed with methanol followed by acetone, and dried using a hot air oven at 300°C. A similar methodology was employed for the synthesis of 2%, 3%, and 4% CdS:Ce nanoparticles.

2.3 Anti-Cancer Activity

The MCF-7 cell line was cultured individually in 96-well plates at a density of 1×10^4 cells per well, utilizing DMEM media supplemented with 1X antibiotic-antimycotic solution and 10% fetal bovine serum (Himedia, India), within a CO_2 incubator maintained at 37°C with 5% CO_2. Doxorubicin was employed as the positive control for comparison purposes.

The cells were subsequently rinsed with 200 μL of 1X phosphate-buffered saline (PBS), after which they were subjected to treatment with various concentrations of nanoparticles in serum-free media and incubated for duration of 24 hours. Following the 24-hour treatment period, the medium was aspirated from the cells. A solution of 0.5 mg/mL MTT, prepared in 1X PBS, was introduced and incubated for 4 hours at 37°C in the CO_2 incubator. Post-incubation, the medium containing MTT was removed, and the cells were washed with 200 μL of PBS. The resulting crystals were then dissolved in 100 μL of dimethyl sulfoxide (DMSO) and mixed thoroughly. The development of color intensity was assessed at a wavelength of 570 nm, with the formazan dye exhibiting a purple-blue hue. Absorbance measurements were taken at 570 nm using a micro plate reader. All experiments were conducted in triplicate. The percentage of cell viability was calculated using the specified equation.

$$\% \text{ Viability} = \frac{\text{Mean OD}_{\text{sample}}}{\text{Mean OD}_{\text{blank}}} \times 100$$

3 Results and Discussion

3.1 Diffuse Reflectance Spectroscopy

Ultraviolet-visible reflectance spectroscopy effectively evaluates CdS particles' optical properties. Bulk CdS exhibits an absorption edge at 515 nm, whereas pure CdS nanoparticles show a band-to-band absorption edge at 541 nm, indicating a notable red shift. This reflects quantum confinement effects typical of nanomaterials and results in a significant decrease in effective band gap energy, emphasizing distinct optical properties that hold crucial implications for optoelectronics and photonics. [13]

The absorption edge of cerium-doped CdS nanoparticles shifts towards the red region as cerium concentration increases compared to pure CdS. This bathochromic shift occurs at wavelengths of 551, 558, 563, and 590 nm for 1%, 2%, 3%, and 4% Ce-doping levels, respectively. This shift is linked to modifications in the band gap, enhancing light absorption capabilities. Cerium integration alters optical properties, affecting absorption onset and adding cerium-related spectral features. Cerium exists in two oxidation states—Ce^{3+} and Ce^{4+}—leading to weaker absorption bands from electronic transitions in the cerium ion, underscoring cerium's importance in semiconductor research and applications.[14]

The Kubelka-Munk plot is a vital tool for analyzing the semiconductor (CdS) in nanocomposites, essential for determining the material's band gap. The K-M function is key in this process, applied to establish the band gap energy (Eg) via Tauc plot analysis. It establishes a relationship between reflectance (R∞), absorption (K), and scattering factors (S) coefficients, expressed mathematically as[15]

$$F(R_\infty) = \frac{(1-R_\infty)^2}{2R_\infty} = \frac{K}{S}$$

This modified function is typically plotted against the photon energy (hv).

$$(F(R_\infty)\,hv)^{\frac{1}{2}}$$

The exponent "n" in the relationship varies with the type of electronic transition. For direct band gap materials like CdS, n equals 2. To determine the band gap value, one must extrapolate the graph's linear section to the energy axis for an accurate representation.

The bandgaps shown in Figure 1 reveal that higher dopant concentrations in CdS nanoparticles lead to a decrease in bandgap energy. This reduction is exclusively linked to the Ce content, not to particle size increases from doping.[16]

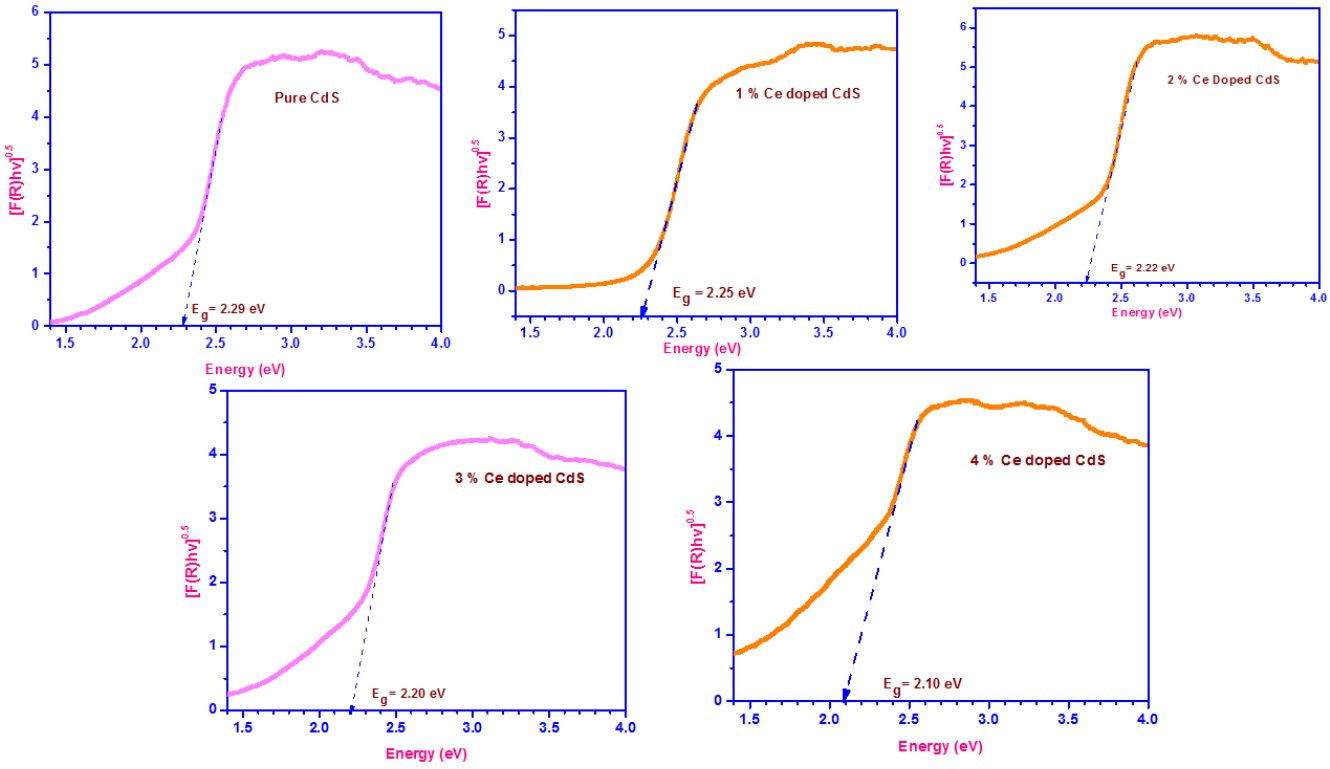

Fig 1. K-M plot of band gap for pure and Ce doped CdS Nanoparticles

3.2 X-Ray Diffraction (XRD) Pattern

The crystalline structure of cerium-doped cadmium sulfide (Ce-doped CdS) nanoparticles was analyzed using X-ray diffraction to assess changes from cerium incorporation. Results showed pure CdS in Wurtzite and Zinc blende forms, with stability

influenced by size and temperature. Adding cerium ions above 2% atomic percentage caused a phase transition from zinc blende to wurtzite, affected by surfactant molecules. The crystalline structure of synthesized CdS nanoparticles was analyzed via X-ray diffraction (XRD). The spectrum reveals peaks of single crystalline Cadmium Sulphide with a zinc blende structure (JCPDS No. 65-2887), confirming high purity. Key 2θ values of 26.40°, 30.26°, 43.56°, and 51.10° correspond to orientations 111, 200, 220, and 311. The predominant (111) peak intensity shows preferential orientation. Doping with Ce ions increases (111) peak intensity and crystallinity, as Ce^{3+} likely substitutes for Cd^{2+} due to similar ionic radii[17]. The average crystallite size was calculated using the Scherrer equation.

$$D = \frac{k\lambda}{\beta cos\theta} \tag{1}$$

For Cubic CdS,

$$\frac{1}{d^2} = \left[\frac{h^2+k^2+l}{a^2}\right] \tag{2}$$

$$a = \frac{\lambda}{2\ Sin\theta}\sqrt{h^2+k^2+l^2} \tag{3}$$

$$V = a^3 \tag{4}$$

For hexagonal CdS,

$$\frac{1}{d^2} = \frac{4}{3}\left[\frac{h^2+hk+h^2}{a^2} + \frac{l^2}{c^2}\right] \tag{5}$$

$$V = \frac{\sqrt{3}}{2}a^2\ c \tag{6}$$

Where D is the crystallite size, K- Scherrer constant (a shape factor 0.94), λ- X-ray wavelength, β - FWHM of the diffraction peak in radians, δ – Dislocation Density, ε –Micro strain, d- inter planar distance, a- lattice Parameter along x axis, c- lattice Parameter along z axis, (hkl) –Miller indices, V- Volume and θ- diffraction angle.

Table 1. Structural parameter of pure and Ce doped CdS Nanoparticles

S. No	Nanoparticles	2θ	FWHM	(hkl)	d_{111} spacing	Lattice parameter (a) nm	Cell volume $(nm)^3$
1	Pure CdS	26.0786	2.2042	(111)	0.3412	0.591	0.2064
2	1 % Ce : CdS	26.3954	2.5190	(111)	0.3371	0.584	0.1992
3	2 % Ce : CdS	26.4520	1.2595	(111)	0.3366	0.583	0.1982
4	3 % Ce : CdS	26.5830	1.5744	(111)	0.3349	0.580	0.1951
5	4 % Ce : CdS	26.7274	3.1488	(002)	0.3331	a = 0.437 c = 0.698	11.0818

3.2.1. Effect of ionic radii influences the lattice parameter of Cerium doped CdS Nanoparticles:

The ionic radius of the dopant ion is crucial for the lattice structure characteristics. Table 1 presents the structural parameters of pure and Ce-doped CdS nanoparticles. Ce^{3+} (1.15 Å) and Ce^{4+} (1.01 Å) have larger radii than Cd^{2+} (0.97 Å), resulting in significant lattice distortion and increased unit cell volume compared to pure CdS nanoparticles.

The increased microstrain becomes evident when substituting Cd with larger dopants like Ce, generating internal stress within the crystalline framework. This stress escalates with higher dopant concentrations due to lattice distortion, highlighting the complexities of mixing different ionic dimensions in solid-state structures[18].

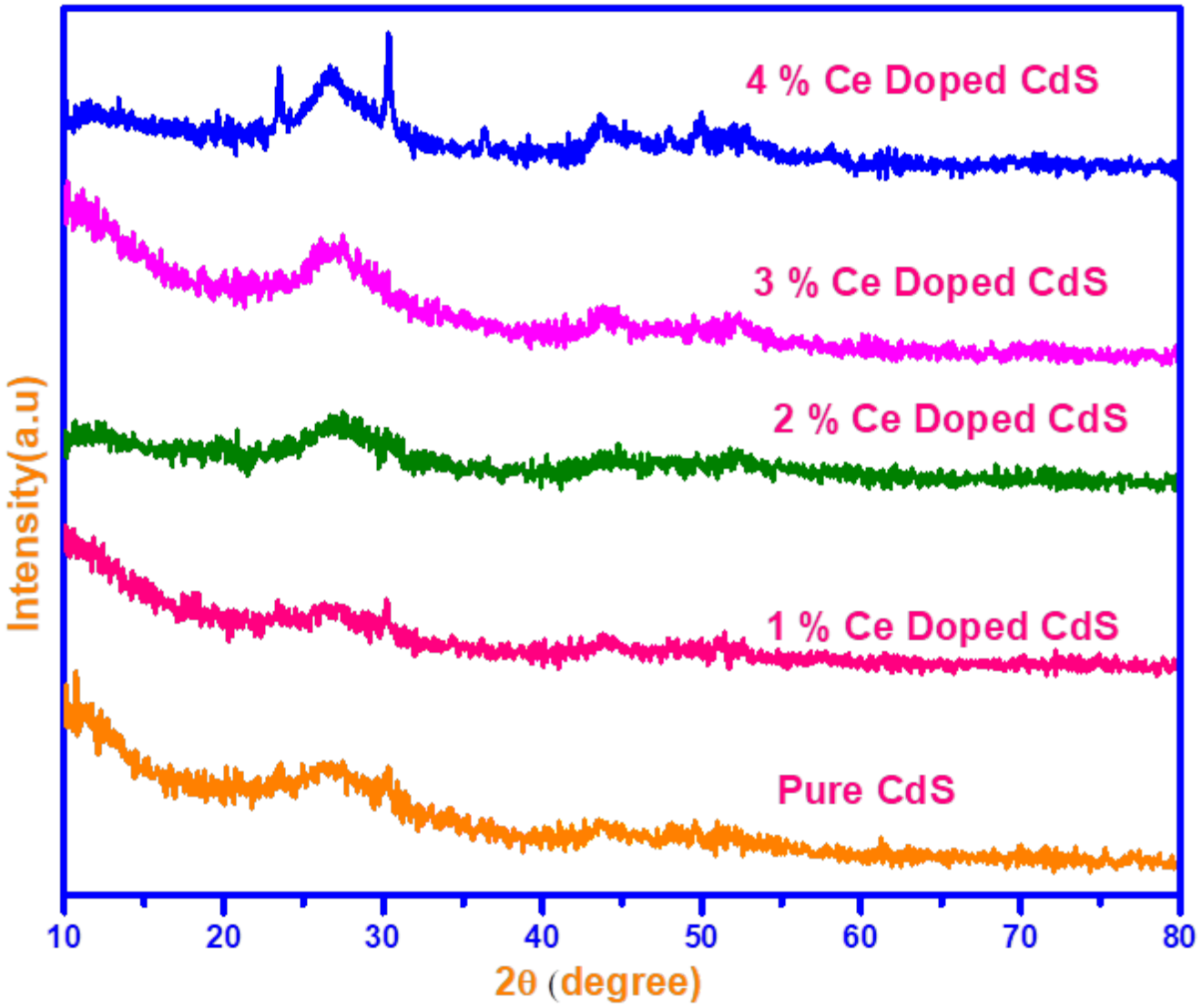

Fig 2. XRD pattern of pure and Ce doped CdS Nanoparticles. Results showed (Fig.2) pure CdS in Wurtzite and Zinc blende forms, with stability influenced by size and temperature.

3.3 Photoluminescence Spectroscopy

Photoluminescence confirms electronic transitions in nanostructured semiconductors. Excitation wavelength affects the emission spectrum. CdS and Ce doped-CdS NPs (Figure 3) show increased intensity with wavelength, peaking at 370 nm. Pure CdS nanoparticles show emission peaks from 440 to 570 nm in their photoluminescence spectra, related to band-edge recombination and surface-trap states. A 450 nm peak indicates direct excitonic recombination, particularly in highly crystalline or small nanoparticles due to quantum confinement. Broader green-yellow emission bands (around 448 nm, 461 nm, 590 nm, and 530-567 nm) are mainly due to intrinsic defects like sulfur and cadmium interstitial vacancies.[19]

Pure CdS nanoparticles exhibit emission peaks from 440 to 570 nm in photoluminescence spectra, linked to band-edge recombination and surface-trap states. A 450 nm peak suggests direct excitonic recombination in highly crystalline or small nanoparticles. Broader green-yellow emission bands (around 448 nm, 461 nm, 590 nm, and 530-567 nm) stem mainly from intrinsic defects such as sulfur and cadmium interstitial vacancies. Defect states, especially sulphur vacancies from cerium ions in the CdS lattice, are linked to red shift and emission. Radiative recombination in these states produces light from new energy

levels. Cerium doping improves emission intensity by altering surface passivation and defect structure, enhancing radiative routes. Luminescence intensity rises with Ce concentration, peaking at 2.3 at% for optimal defect center concentration.

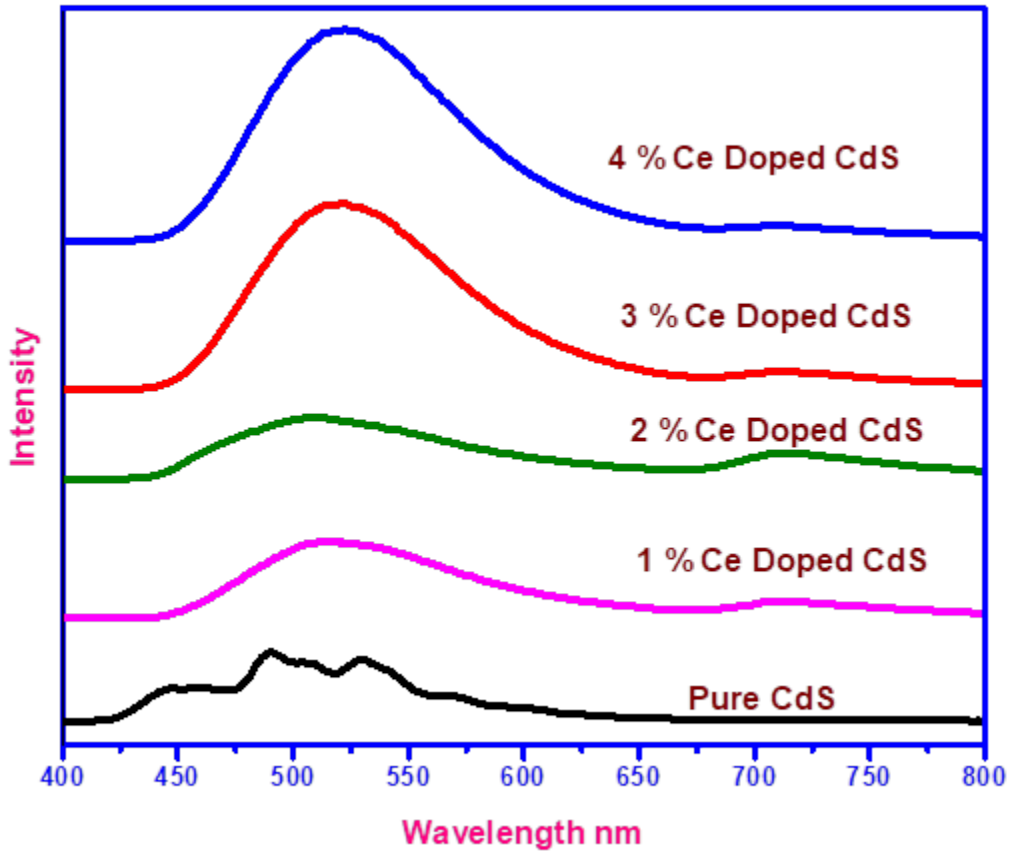

Fig 3. PL spectrum of Pure CdS NPs

3.4 Fourier Transform Infrared Spectroscopy

FTIR spectra are vital for identifying adsorbing chemical species and functional groups in synthesized pure CdS and Ce-doped CdS nanoparticles were shown in Figure 4. These spectra show multiple absorption peaks linked to different vibration modes. Strong bands near 3400 cm^{-1} and 1640 cm^{-1} indicate hydroxyl (–OH) stretching, resulting from absorbed moisture and interaction with water molecules. This understanding is essential for the chemical properties and applications of Ce-doped CdS nanoparticles. For 1%, 2%, 3%, and 4% Ce-doped CdS, a band at 2095 cm^{-1} is noted for C–H stretching, while the N–H asymmetric stretching mode appears near 1515 cm^{-1}, indicating CTAB's presence.[20]

A medium peak around 1402 cm^{-1} may signify the C=O stretching mode linked to the carboxylic group CO2 from the atmosphere. Absorption peaks from 700 cm^{-1} to 500 cm^{-1} correspond to Cd–S stretching modes. Additionally, certain bands near 654 cm^{-1}, 1116 cm^{-1}, 1251 cm^{-1}, and 2095 cm^{-1} diminish as dopant concentration rises, indicating Ce^{3+} ion substitution in the CdS lattice.

3.5 Field Emission Scanning Electron Microscopy

Field Emission Scanning Electron Microscopy (FESEM) offers high-resolution characterization with excellent surface topography. Its field-emission source enhances resolution, enabling detailed nanoscale imaging while minimizing damage to sensitive materials like semiconductors and biomaterials. Low accelerating voltages promote imaging of charging samples in low vacuum, preserving integrity and optimizing secondary electron detection.

FESEM images of Pure CdS NPs and Ce-doped CdS NPs (Figure 5) at 1-4 at.% Ce show distinct characteristics. Pure CdS has undefined grains and compact topography with variable sizes. Doping with 1 at.% Ce produces 5 nm spherical grains[21]

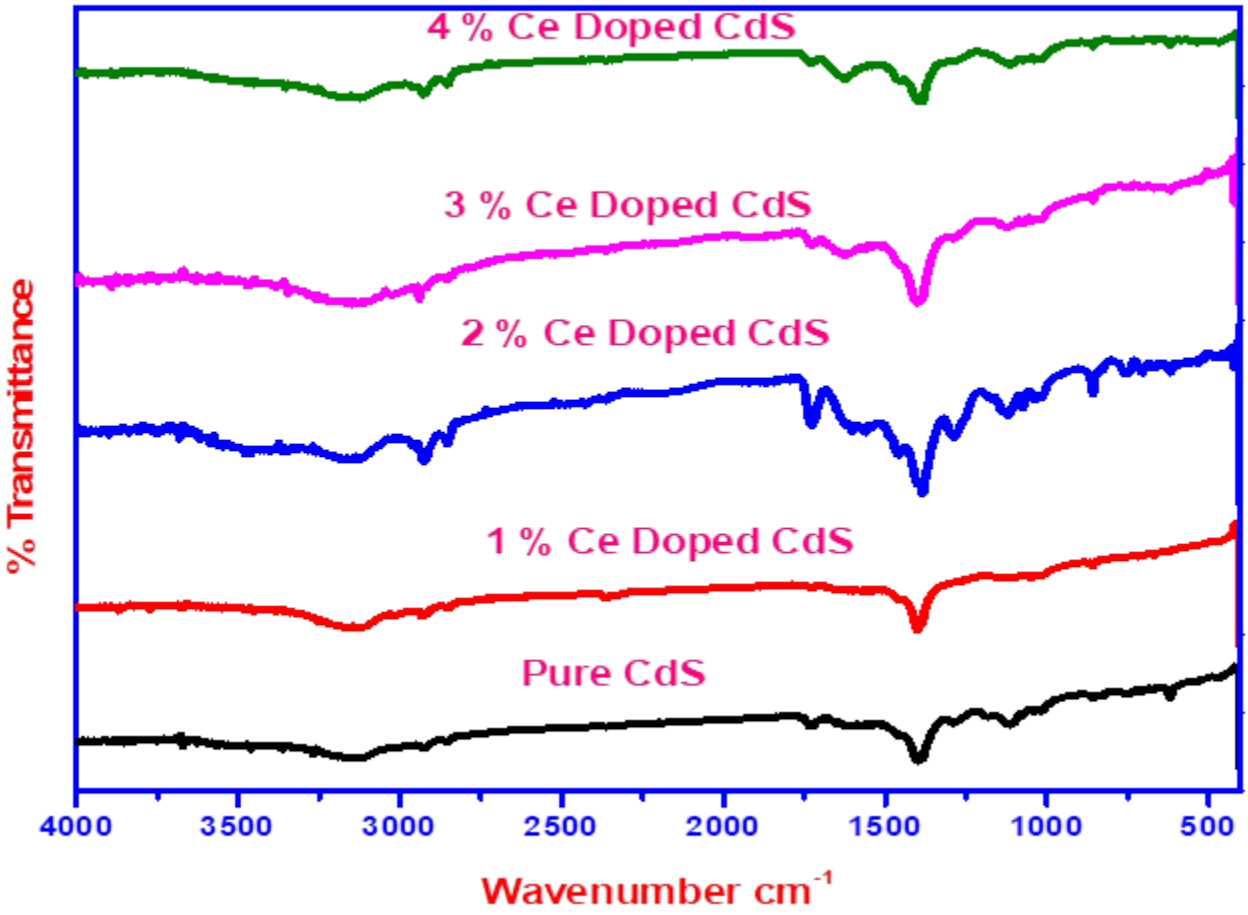

Fig 4. FTIR spectrum of Pure CdS and Ce doped CdS Nanoparticles

and more boundaries. At 2 at.% Ce, a random distribution with sharp-edged grains occurs. 3 and 4 at.% Ce-doped NPs exhibit uniform topography and structural imperfections. Ce-doping alters lattice strain, surface orientation, and defect density, leading to irregular particle shapes but similar surface-to-volume ratios to pure CdS.

3.6 Energy Dispersive X-Ray Analysis

Energy-dispersive X-ray spectroscopy (EDAX or EDS) evaluates the elemental composition of materials, especially nanomaterials. This technique is essential for analyzing the dopant levels in Ce-doped CdS nanoparticles (Figure 6). EDX identified compositions for nanoparticles doped with 1%, 2%, 3%, and 4% cerium nitrate via a surfactant-assisted method. An electron beam stimulates electrons, producing characteristic X-ray emissions: cadmium at 22.1 keV, sulfur at 2.3 keV, and cerium at 5.0 keV, reflecting elemental concentration.

EDAX spectra show Kα peaks for cadmium and sulfur, and a cerium Kα peak confirms cerium in cadmium sulfide.[15] Peak energies align with the Kα transition, and cerium intensity suggests notable incorporation. Carbon peak quantification at 0.3 eV risks overestimations if missed. The spectra verify cadmium, sulfur, and cerium K lines, indicating a high surface presence typical of nanoparticles and good compositional homogeneity.

3.7 Cytotoxic Activity

Nanoparticles exhibit enhanced cytotoxicity due to their small size, high surface-to-volume ratio, and sustained release of therapeutic agents. Clinical studies have assessed the cytotoxicity of CdS and cerium-doped CdS nanoparticles (Ce-doped CdS NPs) on breast cancer cells (**Fig.7,8**). The MTT assay analyzed effects on the MCF-7 cell line at concentrations ranging from 62.50 to 1000 μg/mL, with doxorubicin as control.

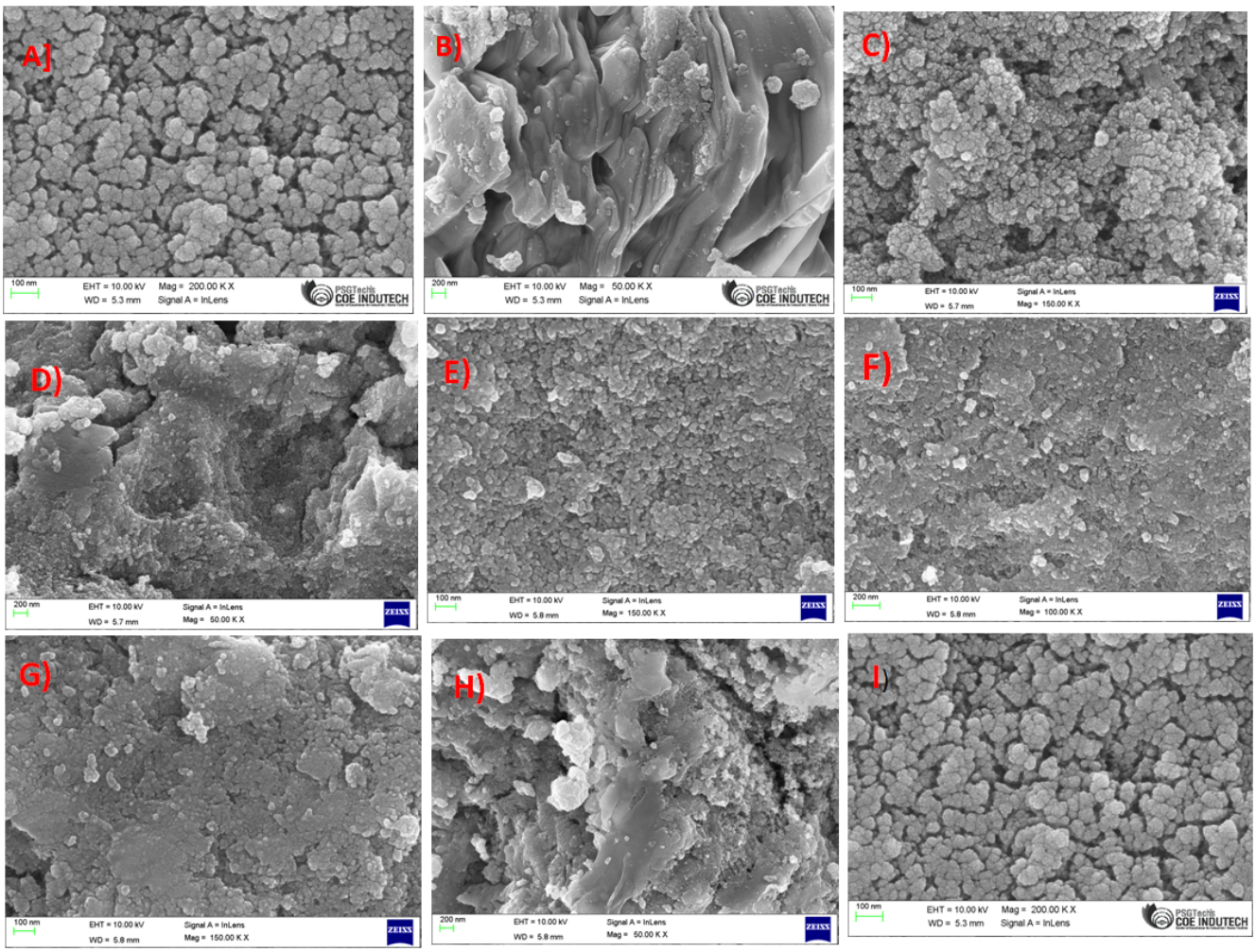

Fig 5. FESEM image of Pure CdS Ce doped CdS NPs [A&B- Pure CdS C&D -1% Ce: CdS, E&F-2% Ce: CdS, G&H- 3% Ce: CdS, I-4% Ce: CdS]

CdS nanoparticles had an IC_{50} value of 179.49 $\mu g \cdot mL^{-1}$, while cerium-doped CdS NPs had IC_{50} values of 382.12, 151.33, 128.61, and 117.31 μg/mL (Table 2) for 1%, 2%, 3%, and 4% inhibitory concentrations. Results suggest significant cytotoxicity of cerium-doped nanoparticles compared to undoped ones, emphasizing their therapeutic potential. Higher Ce-doping improves dispersion and surface area, promoting interaction with cancer cells while maintaining biocompatibility. The relationship between dopant concentration, optical properties, and biocompatibility warrants further investigation to optimize therapeutic efficacy. Enhanced anticancer effects may relate to $Ce^{3+/}Ce^{4+}$ redox cycling, which boosts reactive oxygen species production, underscoring the importance of examining dopant concentration with structural and biological traits for effective cancer therapy development.

3.7.1. Mechanism of Anticancer activity

Cerium-doped cadmium sulfide (CdS:Ce) nanoparticles generate reactive oxygen species (ROS) that induce oxidative stress, important for their anticancer effects. Cadmium and surface oxidation increase superoxide levels in cancer cells, depolarizing mitochondria and activating apoptotic signals, causing apoptosis in mammary and pancreatic cancers. Elevated temperatures further enhance ROS production and cytotoxicity in MCF-7 cells, increasing the effectiveness of the CdS:Ce nanoplatform in promoting apoptosis in breast cancer cells.[22] Surface chemistry influences CdS:Ce nanoparticles' anticancer activity; hydrophobic variants have reduced cellular uptake due to lower membrane interaction and internalization. Biocompatible changes can improve serum protein interaction, enhancing circulation and minimizing aggregation.[23]

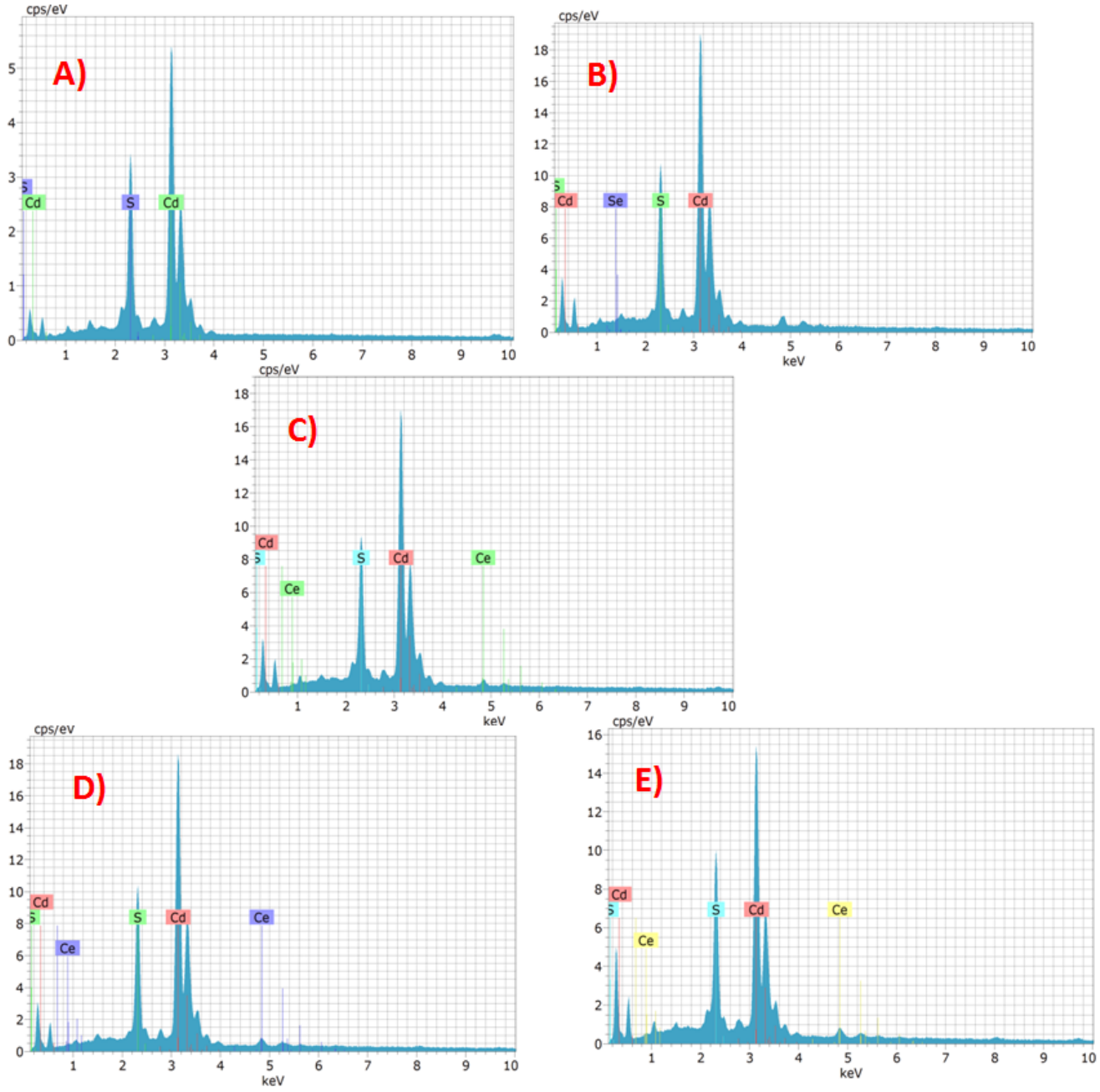

Fig 6. ESAX Spectrum of Pure and Ce doped CdS NPs. A) Pure CdS **B)** 1% Ce : CdS **C)** 2% Ce : CdS **D)** 3% Ce : CdS **E)** 4% Ce : CdS

Free radicals, produced by mitochondria during energy metabolism, can cause cell injury through membrane peroxidation and gene mutations, even under normal conditions. While inhibiting them can be harmful, stressed and cancer cells may produce more. Cerium ion selectively targets cancer cells by reducing free radicals, suggesting possible anti-aging uses in clinical and cosmetic treatments for normal cells.[24]

3.7.1.1. Reactive Oxygen Species Generation and Oxidative Stress. Pure CdS and cerium-doped CdS NPs have anticancer properties. In MCF-7 breast cancer cells treated with CTAB-assisted NPs, Ce:CdS increased lipid peroxidation, leading to mitochondrial disruption, apoptosis, or necrosis. Cerium release may enhance cell death by raising cerium levels, lipid peroxidation, and reducing cytosolic ATP.[23]

3.7.1.2. Mitochondrial Dysfunction and Apoptotic Pathways . Cerium-doped cadmium sulfide (CdS:Ce) nanoparticles induce mitochondrial dysfunction and modify apoptosis in human breast cancer cells. In MCF-7 cells, mitochondrial potential drops significantly after 24 hours, causing increased reactive oxygen species (ROS) and lipid peroxidation. This decline leads to cytochrome c release into the cytosol, resulting in cell death. [25]

3.7.1.3. Ion Release and Cadmium Toxicity Considerations . Ion release from nanoparticles raises concerns, notably cerium-doped cadmium sulfide (CdS), vital due to cadmium's properties. After 24 hours, CdS nanoparticles retained size and shape, releasing minimal cadmium at μg mL^{-1} Cd^{2+} levels. This indicates a lower risk of significant cytotoxicity, highlighting the importance of cerium-doped CdS in safety evaluations. [25]

Table 2. % inhibition of Pure and Ce Doped CdSNPs treated MCF-7 Cells

[NPs] (μg/mL)	Pure CdS	1% Ce : CdS	2% Ce : CdS	3% Ce: CdS	4% Ce : CdS	Doxorubicin
1000	62.29	66.88	90	67.5	84.17	79.79
500	58.85	45.31	75.94	63.23	82.18	75
250	46.88	33.96	74.06	53.23	77.71	56.88
125	38.13	11.88	48.75	38.54	72.19	49.38
62.5	22.19	4.9	27.29	7.81	45.52	46.25

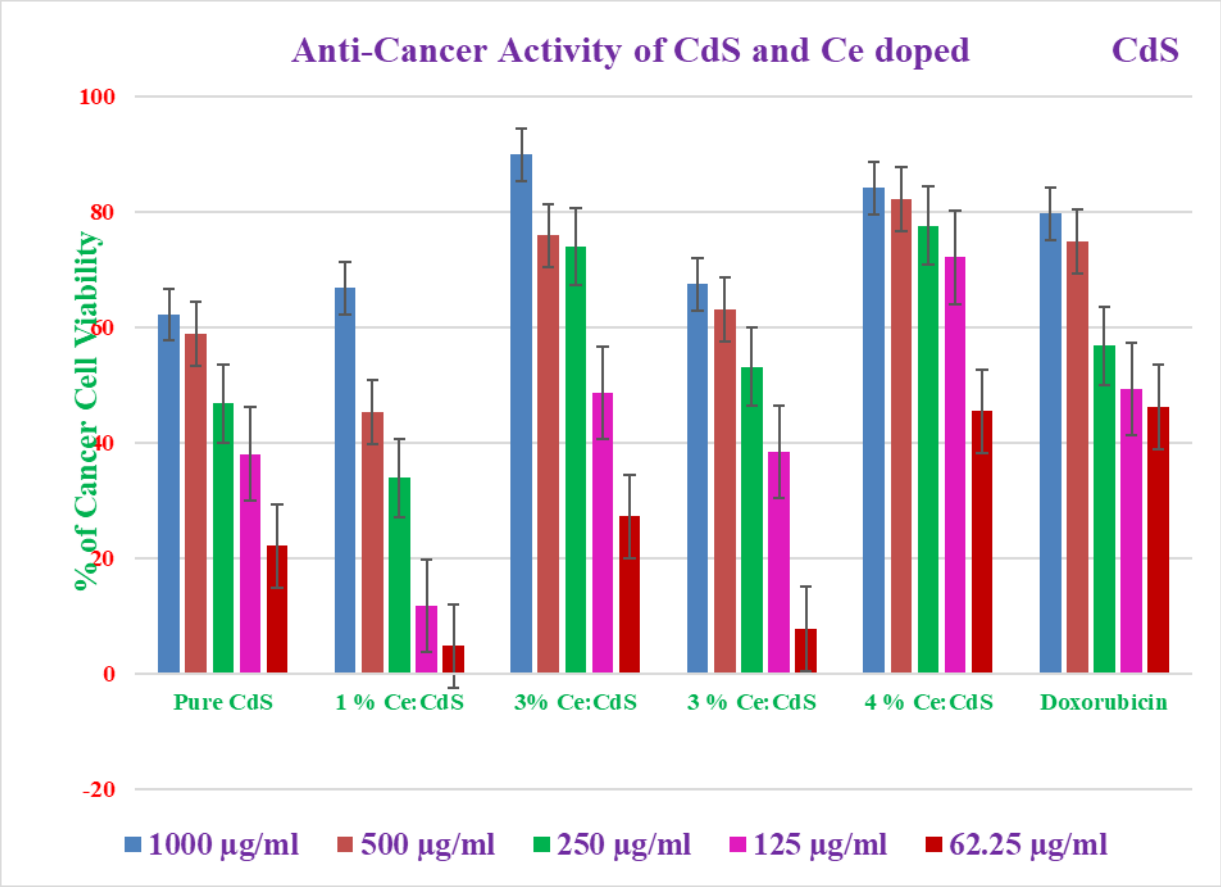

Fig 7. Anti-Cancer cell viability of pure and Ce Doped CdS NPs

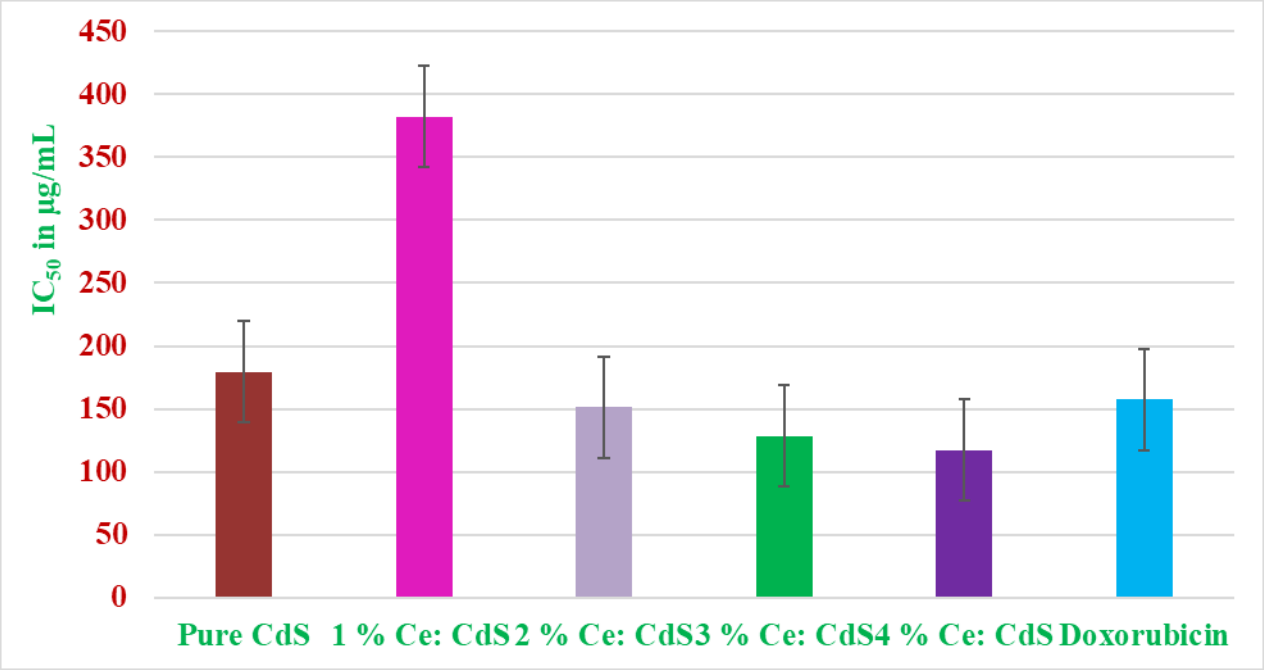

Fig 8. IC_{50} analysis of pure and Ce Doped CdS NPs

4 Conclusion

Pristine CdS nanoparticles were synthesized using a co-precipitation technique, known for its simplicity and cost-effectiveness. Additionally, 1-4% Ce-doped CdS nanoparticles were produced and characterized, showing an increase in crystallite size with Ce doping. The structural, optical, and morphological properties were evaluated, with X-ray diffraction (XRD) revealing the crystalline structure of the CdS powder. The crystalline size for 1-4% Ce-doped CdS ranged from 5 to 25 nm, while pure CdS was 5 nm. Significant impurity levels caused a transition in structure from cubic to hexagonal. UV-Vis measurements indicated the energy bandgap of CdS and Ce-doped CdS was between 2.10 and 2.29 eV, aligning with photoluminescence results. Cerium concentration in the CdS matrix affects peak position and intensity in PL spectra. Lower dopant levels shift band-edge emission to shorter wavelengths, whereas higher levels create defect states that enhance visible emission and broaden spectral features, allowing for tunable photoluminescence in optoelectronic applications. EDAX Spectrum provides crucial evidence of the elemental composition of CdS nanoparticles, revealing Cd and S peaks. Pd doping is indicated by new signals or intensity shifts, confirming successful doping without impurities. This data supports the connection between composition and optical properties, enhancing DRS results for pure and Ce-doped CdS nanoparticles.Field emission scanning electron microscopy (FESEM) analysis showed irregular shapes in spherical-like assemblies. Cytotoxicity assessments revealed that cerium-doped CdS nanoparticles enhance the combat against cancer cell lines by inducing oxidative stress and promoting apoptosis in breast cancer cells, suggesting potential for nanomedicine applications.

5 Acknowledgements

The research received huge support from our Secretary and the Principle of V.O. Chidambaram College in Tuticorin.

References

1) Rasool A, Rizvi TZ, Nayab S, Iqbal Z. Electrical properties of Cadmium Sulfide quantum dots and polyaniline based nanocomposites. *Journal of Alloys and Compounds*. 2021;854(1):156661–156670. https://doi.org/10.1016/j.jallcom.2020.156661.
2) Lee H, Jeong BG, Bae WK, Lee DC, Lim J. Surface state-induced barrierless carrier injection in quantum dot electroluminescent devices. *Nature Communications*. 2021;12(1):5669–5678. https://doi.org/10.1038/s41467-021-25955-z.
3) Jomova K, Alomar SY, Nepovimova E, Kuca K, Valko M. Heavy metals: toxicity and human health effects. *Archives of Toxicology*. 2025;99(10):153–209. https://doi.org/10.1007/s00204-024-03903-2.

4) Savchenko S, Vokhmintsev A, Karabanalov M, Zhang Y, Henaish A, Neogi A, et al. Thermally assisted optical processes in InP/ZnS quantum dots. *Physical Chemistry Chemical Physics*. 2024;26(27):18727–18740. https://doi.org/10.1039/d3cp03931e.
5) Ghasempour A, Dehghan H, Ataee M, Chen B, Zhao Z, Sedighi M, et al. Cadmium Sulfide Nanoparticles: Preparation, Characterization, and Biomedical Applications. *Molecules*. 2023;28:3857. https://doi.org/10.3390/molecules28093857.
6) Patra P, Kumar R, Kumar C, Mahato PK. Ni-incorporated cadmium sulphide quantum dots for solar cell: an evolution to microstructural and linear-nonlinear optical properties. *Journal of Crystal Growth*. 2022;583(1):126542–126555. https://doi.org/10.1016/j.jcrysgro.2022.126542.
7) Singh AK, Vijayashri KM, Singh SP, Mishra MK. Synthesis and characterization of zinc doped cadmium sulphide nanoparticles. *Materials Today: Proceedings*. 2022;66(2):2017–2027. https://doi.org/10.1016/j.matpr.2022.05.484.
8) Xue J, Fujitsuka M, Tachikawa T, Bao J, Majima T. Charge trapping in semiconductor photocatalysts: a time-and space-domain perspective. *Journal of the American Chemical Society*. 2024;146(13):8787–8799. https://doi.org/10.1021/jacs.3c14757.
9) Anand A, Raj A, Mondal D, Maity D, Ganesha MK, Singh AK, et al. Effective Surface Engineering for Defect Passivation and Reduction of Water Oxidation Overpotential in Benchmark 2D α-SnWO4 Nanoplate Photoanodes. *Advanced Functional Materials*. 2024;35(12):2417398–2417407. https://doi.org/10.1002/adfm.202417398.
10) Chen YH, Guan SW, Xing M. Ce-doped defective titanium oxide coating with antibacterial, antioxidant and anti-inflammatory properties for potential application of peri-implantitis treatment. *Rare Metals*. 2025;44(1):472–488. https://doi.org/10.1007/s12598-024-02935-y.
11) Rathore MS, Goyal S, Roopashree R, Parashar K, Sharma K, Grover M, et al. Antibacterial, antifungal, antioxidant and anticancer activities of Sr and Fe doped TiO2 nanomaterial. *Journal of the Indian Chemical Society*. 2025;102(3):101587–101599. https://doi.org/10.1016/j.jics.2025.101587.
12) Hamid MASH, Zengin Y, Boz I. CdxZn1-xS with bulk-twinned homojunctions and rich sulfur vacancies for efficient photocatalytic hydrogen production. *International Journal of Hydrogen Energy*. 2024;52(1):103–114. https://doi.org/10.1016/j.ijhydene.2023.02.067.
13) Zwijnenburg MA. The effect of particle size and composition on the optical and electronic properties of CdO and CdS rocksalt nanoparticles. *Physical Chemistry Chemical Physics*. 2022;24(1):21954–21965. https://doi.org/10.1039/D2CP01342H.
14) Nowsherwan GA, Iqbal MA, Ikram S, Butt AF, Khan M, Ahmad N, et al. Morphological, photoluminescence, and electrical measurements of rare-earth metal-doped cadmium sulfide thin films. *ACS Omega*. 2023;8(39):36321–36332. https://doi.org/10.1021/acsomega.3c04936.
15) Jr L, Salmon, Segundo IR, Freitas E, Vasilevskiy M, Carneiro J, et al. Use and misuse of the Kubelka-Munk function to obtain the band gap energy from diffuse reflectance measurements. *Solid State Communications*. 2022;341(1):114573–114580. https://doi.org/10.1016/j.ssc.2021.114573.
16) Tshikovhi A, Kovhi, Koao LF, Malevu TD, Linganiso EC, Motaung TE. Dopants concentration on the properties of various host materials by sol-gel method: Critical review. *Results in Materials*. 2023;19(1):100447–100458. https://doi.org/10.1016/j.rinma.2023.100447.
17) Mao J, Xu W, Seo S. Exploring the dual phases of cadmium sulfide: synthesis, properties, and applications of hexagonal wurtzite and cubic zinc blende crystal structures. *Journal of Materials Chemistry A*. 2024;12(1):23218–23242. https://doi.org/10.1039/D4TA03496A.
18) Azhar M, Nowsherwan GA, Iqbal MA, Ikram S, Butt AF, Khan M, et al. Morphological, photoluminescence, and electrical measurements of rare-earth metal-doped cadmium sulfide thin films. *ACS Omega*. 2023;8(39):36321–36332. https://doi.org/10.1021/acsomega.3c04936.
19) Wang X, Chen A, Wu XL, Zhang J, Dong J, Zhang L. Synthesis and modulation of low-dimensional transition metal chalcogenide materials via atomic substitution. *Nano-Micro Letters*. 2024;16:163–1–46. https://doi.org/10.1007/s40820-024-01378-5.
20) Fatemipayam N, Keramati N, Ghazi MM. Synthesis and characterization of cadmium sulfide and titania photocatalysts supported on mesoporous silica for optimized dye degradation under visible light. *Scientific Reports*. 2025;15:8160. https://doi.org/10.1038/s41598-025-92077-7.
21) Dutta M, Kalita JM, Wary G. Study of Concentration Quenching and Energy Transfer Mechanism in Ce Doped Y2O3 Nanomaterials. *Journal of Fluorescence*. 2025;3(2):4399–4408. https://doi.org/10.1007/s10895-024-03836-0.
22) Mu T, Zhao C, Wang X, Sun C, He C, Han R. Cerium Nitrogen Co-Doped Carbon Dots Promote Root Growth Of Arabidopsis Thaliana Via Auxin Synthesis And Transport. *Pakistan Journal of Botany*. 2025;57(6):2127–2138. http://dx.doi.org/10.30848/PJB2025-6(16).
23) Amaldoss MJN, Mehmood R, Yang JL, Koshy P, Kumar N, Unnikrishnan A, et al. Anticancer therapeutic effect of cerium-based nanoparticles: Known and unknown molecular mechanisms. *Biomaterials Science*. 2022;10(14):3671–3694. https://doi.org/10.1039/D2BM00334A.
24) Chen Q, Yang X, Yu Y, Duan X, Ni R, Song G, et al. Biomimetic Cerium-Assisted Supra-Carbon Dots Assembly for Reactive Oxygen Species-Activated Atherosclerosis Theranostic. *Small*. 2025;21(8):2408980–2408990. https://doi.org/10.1002/smll.202408980.
25) Cui D, Wang J, Wang H, Yang Y, Zhao M. The cytotoxicity of endogenous CdS and Cd2+ ions during CdS NPs biosynthesis. *Journal of Hazardous Materials*. 2021;409(2):124485–124493. https://doi.org/10.1016/j.jhazmat.2020.124485.